

# Vapour transfer in unsaturated compacted bentonite

P. J. CLEALL\*, R. M. SINGH\* and H. R. THOMAS\*

Results of an experimental and theoretical investigation of heat and moisture movement in unsaturated MX-80 bentonite are presented. A thermo-hydraulic cell that allows measurement of transient temperatures and facilitates the determination of pseudo-transients of moisture content, dry density and chemical composition has been used to perform thermal gradient tests. Results of a number of tests are presented, and observation of the accumulation of chloride ions near the hot end clearly indicates that there is a cycle of vapour and liquid moisture movement, with vapour moving from hotter to cooler regions, condensing, and then moving as liquid towards the hotter regions. An empirical method is applied to calculate approximate vapour fluxes using measured variations in chloride ion concentration and moisture content with time. The vapour fluxes calculated empirically are found to be lower than those determined by some existing vapour flow theories. Subsequently, an existing vapour flow model is modified to represent the observed vapour fluxes more closely.

KEYWORDS: laboratory tests; partial saturation; temperature effects

## INTRODUCTION

Moisture transport in soils under thermal gradients has been a topic of great interest for many years. Problems where thermally induced moisture movement in unsaturated soils is an important phenomenon include performance of buried services (e.g. high-voltage electric cables and hot water pipes), landfill liner performance, optimisation of geothermal energy utilisation (Rees *et al.*, 2000) and thermally enhanced clean-up of contaminated land (Lee *et al.*, 1999). Furthermore, in recent years a great deal of research has been conducted into the disposal of high-level nuclear waste (HLW). In particular, swelling clays have been identified as a candidate material to be used as engineering barriers in deep geological nuclear waste repositories where significant thermal and hydraulic gradients will be present.

Conceptual and theoretical descriptions of moisture movement under thermal gradients have been developed in a number of studies. Early work by Philip & de Vries (1957) developed simultaneous differential equations for the transfer of heat and moisture using numerical data for a coarse-textured and a medium-textured soil that have formed the basis of many subsequent mechanistic formulations. Luikov (1966) applied irreversible thermodynamics to describe liquid and vapour flow, with the resulting formulation having a comparable form to those of Philip & de Vries. A number of researchers have investigated the proposals of Philip & de Vries, leading to various modifications to their original mechanistic formulation: for example, Ewen & Thomas (1989) investigated heating of an unsaturated sand, and concluded that the effective specific area for vapour flow through soil is not a function of air content, and is best represented as being equal to the porosity. Such mechanistic approaches have been used in the development of thermo-hydraulic-mechanical (THM) models (e.g. Thomas & He, 1995; Olivella *et al.*, 1996). Also, the more recent development of THM models to include consideration of chemical species (e.g. Cleall *et al.*, 2007; Gens, 2010) and the signifi-

cant impact of advective processes on chemical transfer necessitates the correct representation of the individual components of moisture movement as well as the net moisture movement. In all such mechanistic models there is the requirement for material parameters to describe the combined influence of various factors such as soil structure, thermal bridging and moisture content. These factors, often given terms such as enhancement, tortuosity or flow area factor, are generally determined empirically via back-analysis of small-scale tests and consideration of the overall moisture flux (e.g. Börgesson *et al.*, 2001; Pintado *et al.*, 2002) and not via consideration of the actual vapour flux, as this is not readily amenable to direct measurement.

Various researchers have carried out laboratory-scale experimental studies of heat and mass transfer in swelling clays subjected to both thermal and hydraulic gradients (e.g. Kanno *et al.*, 1996; Villar *et al.*, 1996; Yong & Mohamed, 1996; Yong *et al.*, 1997; Pintado *et al.*, 2002; Gatabin & Billaud, 2005; Villar *et al.*, 2008; Gómez-Espina & Villar, 2010), and also of the thermal properties of swelling clays (e.g. Madsen, 1998; Tang *et al.*, 2008). Although they yielded high-quality data, and were able to quantify overall moisture movement, none of these studies has been able to quantify the individual vapour flux component. However, recently Cleall *et al.* (2011) have presented an empirical method that allows the vapour flux component to be estimated via consideration of the net moisture flux and the movement of a conservative soluble ion.

The aim of this paper is to quantify the individual component of vapour fluxes due to applied thermal gradients in a swelling soil. Results from a series of tests on MX-80 bentonite are presented, and then the empirical method of Cleall *et al.* (2011) is applied to calculate vapour fluxes via consideration of variations of soluble chloride ion concentration and moisture content with time. The empirically calculated vapour fluxes are compared with those determined by existing vapour flow theories, and finally a modified vapour flow model is presented.

## TEST METHODOLOGY AND MATERIAL

MX-80 bentonite, a montmorillonite-rich swelling clay, was chosen as the test material, owing to its potential use as a buffer material in HLW repositories. This material has

Manuscript received 1 October 2012; revised manuscript accepted 5 February 2013. Published online ahead of print 18 April 2013. Discussion on this paper closes on 1 February 2014, for further details see p. ii.

\* Geoenvironmental Research Centre, Cardiff School of Engineering, Cardiff University, Wales, UK.

been selected for both its swelling properties and its high sorption capacity (Börgesson *et al.*, 2001) as the candidate buffer material in a number of European HLW waste disposal programmes. The MX-80 was supplied in a powdered form, oven-dried (at 105°C) for 24 h, and then mixed with water to ensure uniform distribution of moisture.

The MX-80 bentonite tested has been characterised by determining various geotechnical, physical and chemical properties, a summary of which is presented in Table 1; full details of their determination are given in Singh (2007). In this study, a target dry density of 1.65 Mg/m<sup>3</sup> has been selected for the initial condition of the material with two possible initial water contents (16% and 22%), thereby allowing two types of sample to be considered, termed hereafter ‘wet samples’ and ‘dry samples’. The initial degree of saturation of the wet and dry samples was 88% and 60% respectively.

In the tests reported here, cylindrical samples (100 mm high and 100 mm in diameter) were subjected to a fixed thermal gradient within a sealed cell (Fig. 1). This cell, full details of which have been presented elsewhere (Singh, 2007; Cleall *et al.*, 2011), allows varying thermal boundary conditions to be applied longitudinally to sealed and fully constrained cylindrical clay samples. The soil samples were statically compressed in layers in the central section of the cell by using a specifically designed and built rammer. The compaction method consisted of compression of the soil samples in ten layers under a maximum static load up to 90 kN with a loading and unloading rate of 1.5 kN/s. Fig. 2 shows typical water content and dry density profiles with the depth of the soil samples achieved after an equilibrium period of 24 h. The initial state of the specimens was determined from samples prepared following the same methodology, including the equilibration period. Longer equilibrium periods of 1–5 days were also tested, with no

**Table 1. Properties of MX-80 bentonite**

Property		Value
Natural water content: %		12–14
Specific gravity		2.80
Liquid limit: %		385
Plastic limit: %		39
Plasticity index: %		346
Activity: %		3.46
Linear shrinkage: %		42
Swell index: ml/2g		32
pH	(soil water ratio 1:10)	9.20
	(soil water ratio 1:15)	9.28
Specific surface area (EGME method): m <sup>2</sup> /g		650
Initial ion concentration Cation exchange capacity	Chloride: mmol/kg	2.92
	Sodium: meq/100 g	53.08
	Magnesium: meq/100 g	7.83
	Potassium: meq/100 g	1.07
	Calcium: meq/100 g	31.00
	Total: meq/100 g	92.88
Mineral composition by X-ray diffraction (XRD)	Montmorillonite: %	78
	Albite: %	10
	Quartz: %	11

significant variation found in the profiles of porosity, moisture content or chemical composition.

The samples were subjected to fixed temperatures of 85°C at the bottom end and 25°C at the top end, resulting in an average thermal gradient of 0.6°C/mm. A series of tests have been undertaken, each with different durations (e.g. 1, 3, 7, 15 and 30 days) to provide pseudo-transient data for both the

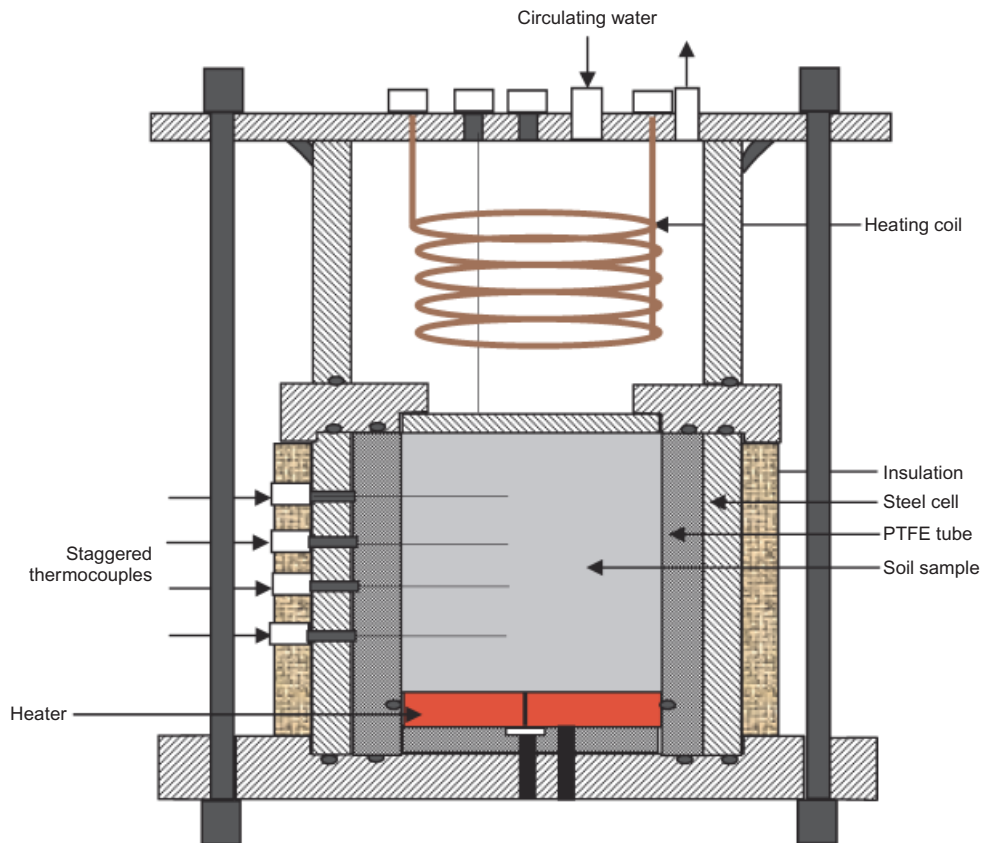


**Fig. 1. Test cell**

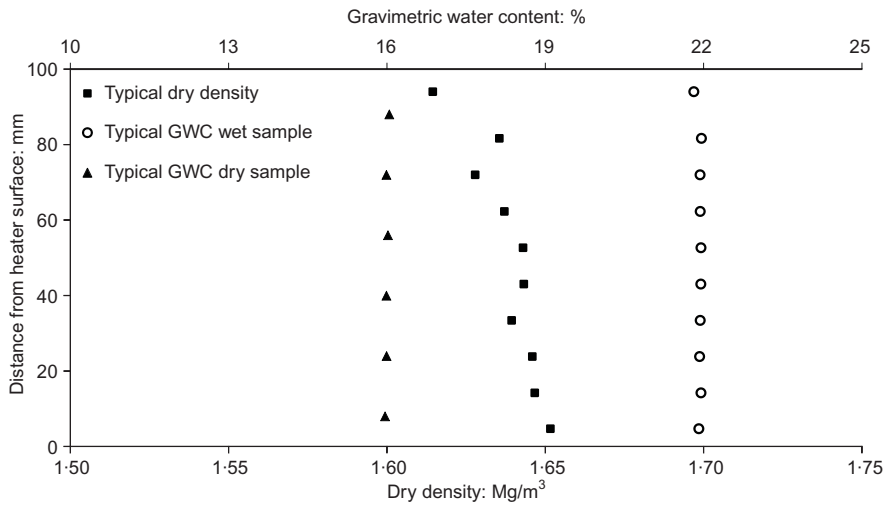


Fig. 2. Typical initial gravimetric water content and dry density variation

wet and dry samples. At the end of each test the samples were sliced into ten sections, each approximately 10 mm thick, with moisture content, porosity and ion concentration determined. Moisture content and porosity were determined following BS 1377-2 (BSI, 1990). The specimens were prepared for chemical analysis following US EPA 1312 (US EPA, 1994), with dried and crushed soil samples diluted with deionised water to a solid:water ratio of 1:20. Chemical concentration data were obtained via inductively coupled plasma mass spectroscopy (ICPMS). Aqueous extract concentrations were then converted to chemical concentrations in terms of mol/kg (by mass of dry soil), presented below. Where a number of measurements of a parameter were taken for a slice, the average of these values is presented. Consideration of the moisture content and porosity allows conversion to concentrations, in terms of mg/l (chemical mass to pore water volume), that are required for the vapour flux calculations described below.

EXPERIMENTAL RESULTS

The temperature, moisture content, porosity and chemical concentration data of each test are presented in Figs 3–10 and discussed below in turn.

Dry sample

In both the dry and wet sample thermal equilibrium was achieved within 4 h, reflecting the highly constrained boundary conditions applied to the thermal field. Thermal profiles

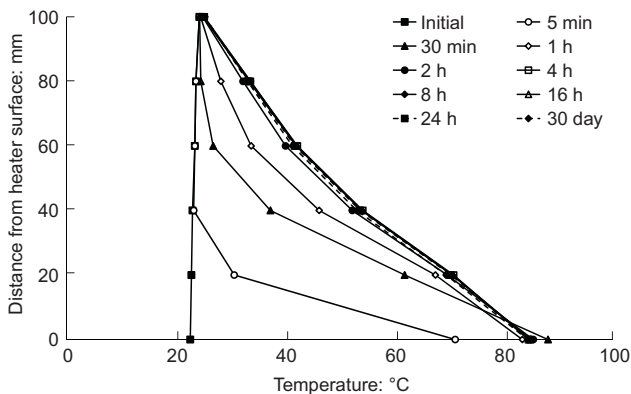


Fig. 3. Temperature profile of dry sample for temperature gradient test

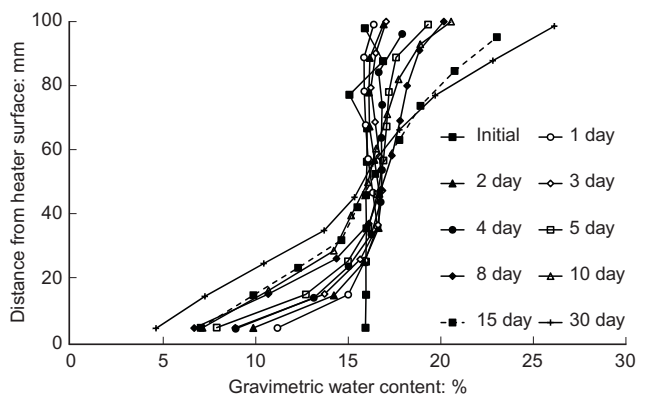


Fig. 4. Gravimetric water content distribution of dry sample for temperature gradient test

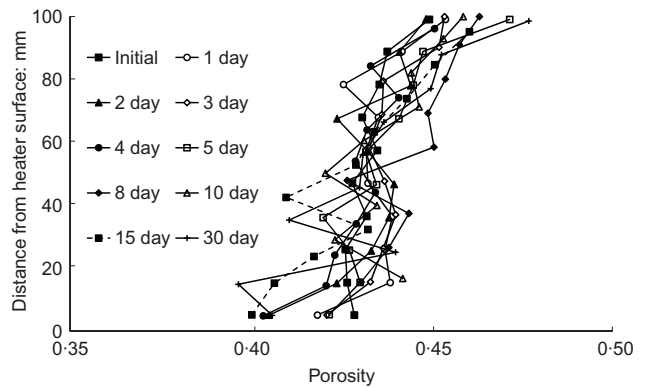


Fig. 5. Porosity profile of dry sample for temperature gradient test

within the dry sample are shown in Fig. 3; at steady state the temperature gradient varies from 0.76°C/mm near the heater surface to 0.425°C/mm near the cold end. This variation in thermal gradient is likely to be due to a combination of three factors: changes in thermal conductivity due to moisture content and dry density variations, heat loss through the walls of the cell and advective movement of latent heat.

The gravimetric water content variation at various time intervals for the dry sample is shown in Fig. 4. The initial water content is relatively uniform throughout the sample length. In general, it can be seen that the gravimetric water

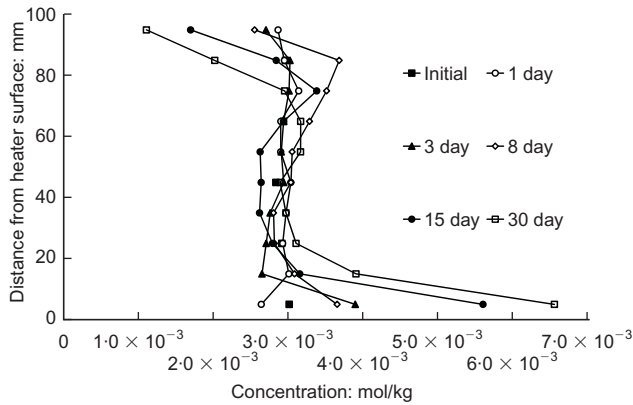


Fig. 6. Soluble chloride distribution of dry sample for temperature gradient test

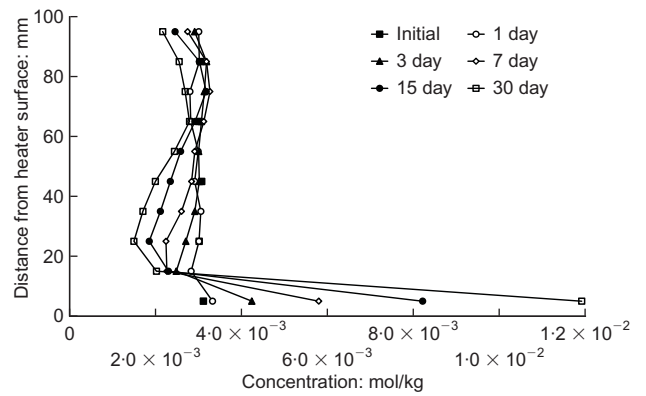


Fig. 10. Soluble chloride distribution of wet sample for temperature gradient test

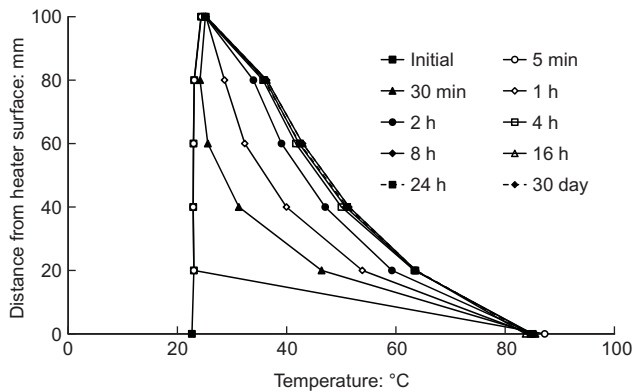


Fig. 7. Temperature profile of wet sample for temperature gradient test

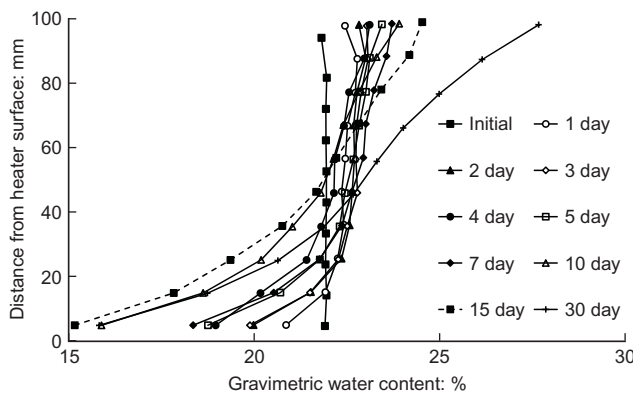


Fig. 8. Gravimetric water content distribution of wet sample for temperature gradient test

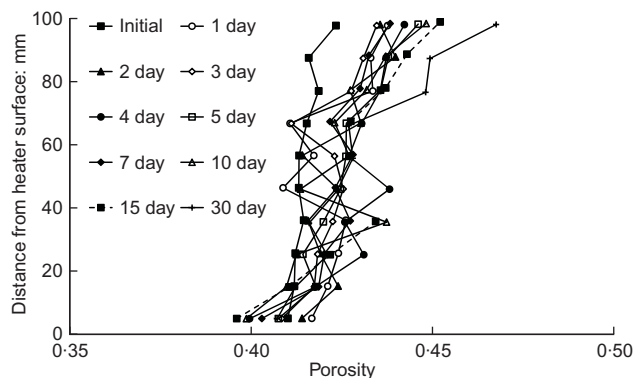


Fig. 9. Porosity profile of wet sample for temperature gradient test

content decreases near the heater surface and increases near the cold end with time. It is apparent that the temperature gradient within the sample causes an overall movement of moisture towards the cooler end of the sample, with the test results at 30 days showing drying in the bottom half of the sample while the top half is experiencing localised wetting. During the test the drying front (marking the interface between the region that has undergone drying and the region at or above the initial moisture content) progressively moved towards the mid-height of the sample. At the end of each experiment mass balance was checked and found to be within  $\pm 0.2\%$ , which indicates no significant mass loss from the cell.

The porosity variation with time for the dry samples is presented in Fig. 5. Although the data are quite noisy, it can be observed that, in general, the porosity is decreasing near the hot end, indicating drying-related shrinkage, and increasing near the cold end, indicating wetting-related swelling, for example by comparing initial and 30 day profiles. No development of a gap between the sample and cell wall was observed at the end of any of the tests. The initial porosity, along with the data shown in Fig. 2, indicates a relatively uniform and homogeneous sample.

Soluble chloride concentration profiles are shown in Fig. 6, with an overall trend of increasing concentration near the heater surface and decreasing concentration in the cooler regions. As the soluble chloride ions can only be carried advectively or move diffusively – in other words, soluble chloride can only move in the liquid phase while it cannot be transported in the vapour phase that moves towards cooler zones – the increase in soluble chloride ion concentration near the heater surface indicates a movement of liquid moisture towards the hot end, owing to suction gradients towards the heater surface. The progressive accumulation of soluble chloride ions near the hot end indicates that a cycle of vapour and liquid moisture movement within the soil sample has developed, with moisture moving away as vapour from the hot end, condensing in cooler regions, and then flowing back towards the hot end as liquid.

*Wet sample*

The steady-state temperatures at each point within the wet samples are lower than in the dry samples, owing to an increased variation in temperature gradient, as can be observed in Fig. 7. The temperature gradient is  $1.08^\circ\text{C}/\text{mm}$  near the heater surface and  $0.56^\circ\text{C}/\text{mm}$  near the cold end. It appears that higher variations in thermal conductivity are present in the wet sample, as any radial heat loss from the cell wall would be expected to be similar for each of the tests.

The gravimetric moisture content results for the wet sample at various time intervals are presented in Fig. 8. As with the dry sample, the water content is progressively decreasing at the hot region and increasing at the cold region, with the drying almost reaching the mid-height of the sample after 15 days. It can also be seen that equal quantities of localised drying and wetting are measured at either end of the sample after 30 days. Mass balance checks at the end of each test found that in the entire test series negligible moisture loss occurred.

Porosity profiles for the wet samples at various times are shown in Fig. 9. As with the dry sample, the porosity is decreasing near the heater surface, owing to drying-related shrinkage, and increasing in the cooler, wetter regions.

Figure 10 presents the soluble chloride ion concentration distribution through the sample at various times. As with the dry sample, the overall trend is one of increasing concentration near the heater surface and decreasing concentration in the colder regions. Comparison with the variations in moisture content shown in Fig. 8 again indicates soluble chloride ions being advectively carried by the liquid moisture to the hot end. In comparison with the dry sample results, the soluble chloride ion concentration is higher near the heater surface for the wet samples. This greater accumulation in the wet sample is possibly due to larger quantities of water transport and therefore movement of soluble chloride.

In summary, the moisture content progressively decreases in the warm region and increases in the cool region with time, irrespective of different initial conditions. In both cases the porosity is observed to increase in the cool region and decrease in the hot region. Soluble chloride ion accumulation near the heater surface, probably resulting from advective movement of this conservative ion, indicates that moisture moves away from the warmer regions in the vapour phase and then condenses in the cooler regions, with a subsequent movement of liquid back towards the warmer regions.

#### EMPIRICAL QUANTIFICATION OF VAPOUR FLUX

An empirical calculation is used to determine the vapour flux from measured soluble chloride ion concentrations and moisture contents for each slice, and is based on the assumption that advection towards the hot end is the dominant process occurring in the soil in the time period considered, and that diffusion processes are small and can be ignored. This follows the approach presented by Cleall *et al.* (2011), which was applied to a slightly swelling kaolin. Here the chloride ion is selected, as it is a conservative negative ion and would be expected to move advectively with bulk liquid moisture, and as the chloride movement is not affected by the negative charge of the clay particles little or no retardation will occur.

The method assumes that the soil sample consists of a vertical stack of layers, and that a thermal gradient is applied along the soil sample, with the higher temperature at the bottom end and the lower temperature at the top end. The bottom layer (first layer) initially (at time  $t = t_1$ ) has a mass of chloride ions of  $m_1^{t_1}$  (in mg). After the start of the test, the first layer has an influx of chloride ions carried by liquid moisture from the next layer (layer 2). At any time ( $t = t_2$ ), the mass of chloride ions in the first layer is  $m_1^{t_2}$ . The change in mass of chloride ion,  $\Delta m_1$ , in the first layer can be determined as

$$\Delta m_1 = m_1^{t_2} - m_1^{t_1} \quad (1)$$

$\Delta m_1$  is the mass of chloride that has entered the first layer from the second layer with liquid moisture. The concentration of chloride ions in the second layer is known at both

$t = t_1$  and  $t = t_2$ . The chloride ions will move with liquid moisture to the first layer from the second layer with the existing concentration in the second layer. Therefore the amount of liquid moisture,  $\Delta V_{\text{liq}(2 \rightarrow 1)}$  (in ml), moving with chloride ions from the second layer to the first layer can be calculated, assuming a linear transient variation of concentration, as

$$\Delta V_{\text{liq}(2 \rightarrow 1)} = \frac{\Delta m_1}{C_{2m}} \quad (2)$$

where

$$C_{2m} = \frac{C_2^{t_1} + C_2^{t_2}}{2} \quad (3)$$

$C_{2m}$  is the average chloride concentration (in mg/l) in the second layer during the time interval considered (i.e.  $t = t_1$  to  $t = t_2$ ),  $C_2^{t_1}$  is the initial chloride concentration in the second layer at time  $t = t_1$ , and  $C_2^{t_2}$  is the chloride concentration in the second layer at time  $t = t_2$ .

The liquid moisture,  $\Delta V_{\text{liq}(2 \rightarrow 1)}$ , comes into the first layer from the second layer and adds to the existing initial moisture,  $V_1^{t_1}$ , of the first layer. Therefore the new liquid moisture in the first layer at time  $t = t_2$  can be expressed as

$$V_1^{t_2} = V_1^{t_1} + \Delta V_{\text{liq}(2 \rightarrow 1)} - \Delta V_{\text{vap}(1 \rightarrow 2)} \quad (4)$$

where  $\Delta V_{\text{vap}(1 \rightarrow 2)}$  is the amount of vapour moisture moving from the first layer to the second layer. As the initial and final moisture quantities are measured experimentally, and  $\Delta V_{\text{liq}(2 \rightarrow 1)}$  is determined from equation (2), the amount of vapour movement from the first layer can be determined. Therefore the vapour flux,  $q_{(1 \rightarrow 2)}$ , across the interface between the first and the second layer can be found. This calculation can then be repeated for each interface, moving up through the sample slice by slice. For the remaining layers, movement of liquid moisture out of the layer should also be considered, resulting in a more general form of equation (2) of

$$\Delta V_{\text{liq}(n \rightarrow n-1)} = \frac{\Delta m_1 + C_{(n-1)m} \Delta V_{\text{liq}(n+1 \rightarrow n)}}{C_{(n)m}} \quad (5)$$

Finally, it should be noted that these calculations have been performed in terms of a normalised layer volume to account for any variation in layer thickness.

This method can be applied only to sealed thermal tests, and is dependent on a number of limiting assumptions related to advection being the overwhelmingly dominant mechanism for soluble chloride ion movement, a linear transient variation of concentration within a layer during a time step, and the fact that no appreciable volume change occurs in the samples between extraction and initial measurement. This method should therefore be considered to yield an approximation to the vapour flux; however, it is claimed that it does give a valuable quantification of the vapour flux component.

Figures 11 and 12 show the empirically approximated average vapour fluxes at the interfaces of each of the sampled slices for the dry and wet samples respectively for each of the periods. Some interesting patterns of behaviour can be observed.

During the initial period (0–3 days), a similar trend of higher fluxes at the hotter end is observed in both cases, with slightly higher fluxes calculated for the dry sample. Also, during these initial 3 days (0–3 days), peak vapour fluxes are estimated in the hot region of the dry sample. In this period, thermal equilibrium is attained largely after 4 h; also, in these early stages the situation may be further complicated by an initial liquid moisture movement due to

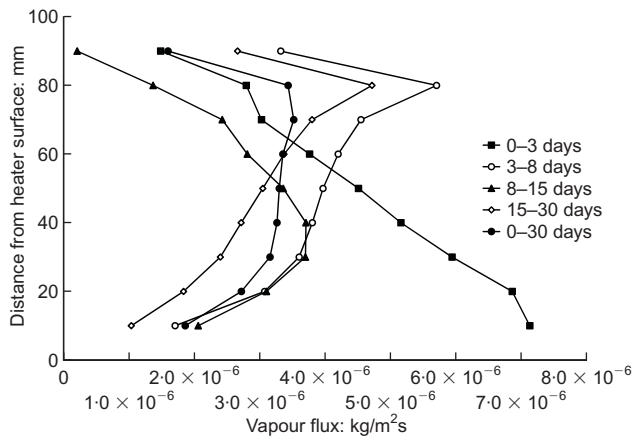


Fig. 11. Calculated vapour flux of dry sample for temperature gradient test

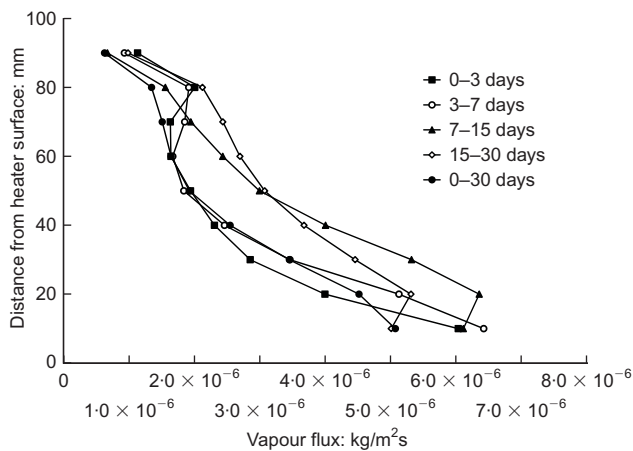


Fig. 12. Calculated vapour flux of wet sample for temperature gradient test

changes in suction caused by the change in thermal regime, away from the heater.

From 3 days onwards a distinctly different response is observed between the two samples. The wet sample exhibits very similar profiles of vapour flux for the periods 3–7, 7–15 and 15–30 days, which are also similar to the overall average for the 0–30 day period and the 0–3 day period. These remarkably steady values imply that from a very early stage the vapour flux has become established and stable throughout the sample. In the dry sample the flux profile changes dramatically from the 3–8 day period onwards, with a distinct drop in flux levels in the hotter layers leading to a system where the vapour flux is higher in the cooler regions in the 3–8, 8–15 and 15–30 day periods. Interestingly, a similar drop in vapour fluxes after an initial period was reported by Cleall *et al.* (2011) for a sample of kaolin at a similar initial moisture content and dry density. As with the wet sample, the system appears to be tending towards a state of relatively stable vapour fluxes. The 0–30 day period results for the dry sample give a representation of the overall vapour movement within the system, with lower fluxes in both the hot dry region and the cool wet region.

COMPARISON WITH THEORETICAL MODELS OF VAPOUR FLUX

Many theoretical models of diffusive vapour flux find their origins in the work of Philip & de Vries (1957), who presented a vapour flow equation with the general form

$$q_v = -D_{atms} \nu_v \tau_v \theta_a \nabla \rho_v \tag{6}$$

where  $\nu_v$  is a mass flow factor equal to the ratio of the partial pressure of the air fraction to the total gas pressure,  $\tau_v$  is a tortuosity factor,  $\theta_a$  is the volumetric air content,  $\rho_v$  is the vapour density, and  $D_{atms}$  is the molecular diffusivity of vapour through air, which can be described by

$$D_{atms} = 2.2 \times 10^{-5} \left( \frac{P_{atm}}{P_g} \right) \left( \frac{T}{T_0} \right)^{1.75} \tag{7}$$

where  $P_{atm}$ ,  $P_g$ ,  $T_0$  and  $T$  are the atmospheric pressure, the pore gas pressure, the reference temperature and the temperature respectively. In some approaches (e.g. Philip & de Vries, 1957; Ewen & Thomas, 1989) the vapour flux is separated into two components by considering the dependence of vapour density on temperature and moisture content, to give

$$\nabla \rho_v = \left( h \frac{\partial \rho_0}{\partial T} + \rho_0 \frac{\partial h}{\partial T} \right) \nabla T + \rho_0 \frac{\partial h}{\partial \theta} \nabla \theta \tag{8}$$

where  $\rho_0$  is the saturated vapour density,  $\theta$  is the volumetric moisture content, and  $h$  is the relative humidity, which can be defined by a thermodynamic relationship proposed by Edlefsen & Anderson (1943) as

$$h = \exp \left( \frac{\psi g}{R_v T} \right) \tag{9}$$

where  $\psi$ ,  $g$  and  $R_v$  are the capillary potential, the gravitational constant and the specific gas constant for vapour respectively.

To allow comparison of the experimentally estimated vapour fluxes with the theoretical predictions, it is necessary to establish a soil water retention curve. A series of filter paper technique tests, using the non-contact filter paper technique, have been undertaken, at a constant temperature of 20°C on samples initially at the reference target dry density of 1.63 Mg/m<sup>3</sup> and in a wet condition, and the obtained experimental data fitted to the van Genuchten (1980) model

$$S_{le} = \frac{S_l - S_{lr}}{S_{ls} - S_{lr}} = \left[ 1 + \left( \frac{s}{P_0} \right)^{1/(1-\lambda)} \right]^{-\lambda} \tag{10}$$

where  $S_{le}$  is the effective degree of saturation,  $S_{lr}$  is the residual degree of saturation,  $S_{ls}$  is the maximum degree of saturation,  $s$  is the suction (in MPa), and  $\lambda$  and  $P_0$  are fitting parameters. The values for these parameters are given in Table 2, and the fitted curve and data are shown in Fig. 13. As suggested by Thomas & Sansom (1995), consideration of the surface energy of soil water,  $\xi$ , using the Edlefsen & Anderson (1943) surface energy function, allows application of the moisture retention curve at different temperatures (curves at various temperatures are shown in Fig. 13).

Using experimentally measured data at 30 days to describe the variation in temperature, moisture content and porosity within the sample, equations (8)–(10) can be applied to

Table 2. Parameters for soil water retention curve

Parameter	Value
$S_{lr}$	0.0
$S_{ls}$	0.92
$\lambda$	0.375
$P_0$ : MPa	21.8

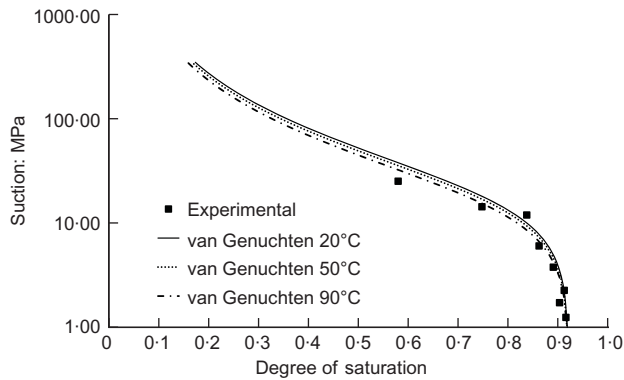


Fig. 13. Soil water retention curve

provide estimates of the gradient of vapour density within each of the samples. Combining these estimates with the Philip & de Vries vapour flow equation (equation (6)) yields the theoretical predictions of vapour flux shown in Figs 14 and 15. The value of the tortuosity factor  $\tau_v$  has been set to 0.5, using a least-squares regression, to achieve the closest overall representative fit to the experimentally estimated vapour fluxes. In making this comparison, vapour movements due to total pore air pressure gradients have been ignored. Previous assessments of such systems (e.g. Thomas & Sansom, 1995) have found that, owing to the relative ease of bulk pore air movement and subsequent equilibration, such impacts at this scale are likely to be limited. Also, it is reasonable to assume that any pressure-gradient-driven flow

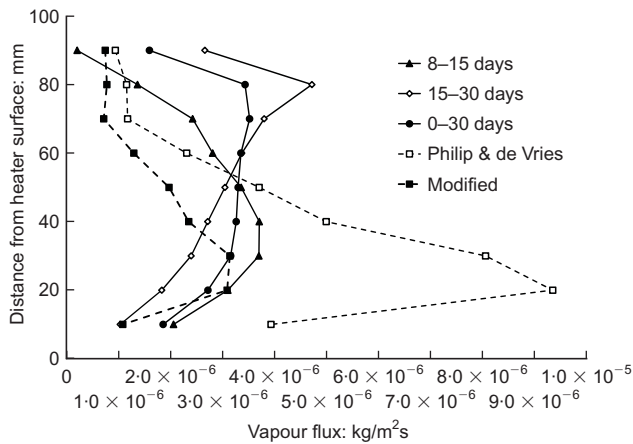


Fig. 14. Theoretical vapour fluxes for dry sample

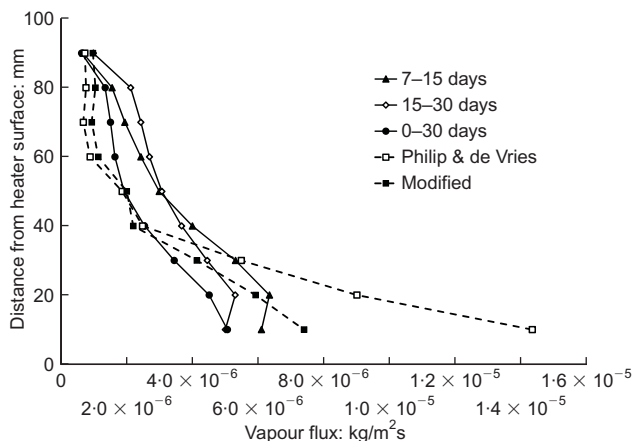


Fig. 15. Theoretical vapour fluxes for wet sample

component, due to differential increases in air pressure resulting from heating, would become relatively small once the initial heating phase had passed (within the first 4 h) and the air pressures had been able to equilibrate; Olivella & Gens (2000) also offer a useful investigation of these issues. It can clearly be seen that in both the dry and wet samples the fluxes are being overestimated in the lower, hotter and drier, regions.

It is apparent that in the drier regions the vapour flux is significantly lower than that predicted by the Philip & de Vries vapour flow equation. Considering the terms in this equation that were originally introduced to represent the impact of the porous materials on vapour flow, the mass flow factor and volumetric air content both increase in the lower regions of the sample, while the tortuosity factor remains constant. It is apparent that the mass flow factor and volumetric air content are not representing the measured variations in vapour flux. In some ways this is not entirely surprising, as these are essentially empirically based factors that have been developed largely on the basis of the behaviour of coarse-grained, non-swelling soils. As a purely empirical step these two variable terms have been replaced by the porosity, yielding the equation

$$q_v = -D_{atms} \tau_v n \nabla \rho_v \tag{11}$$

The porosity  $\tau_v$  component of the volumetric air content term has been retained to allow variations in density to continue to be represented. Modified theoretical predictions using this equation and a revised value of the tortuosity factor  $\tau_v$  of 0.11, to achieve the closest overall representative fit, via a least-squares regression, are shown in Figs 14 and 15. A considerably closer fit to the experimentally estimated fluxes can be seen for both the samples. This approach – to assume that the vapour flow area is equal to the porosity, and that there is no choking – follows that reported previously by Ewen & Thomas (1989) for a medium sand. It is recognised that these modifications are empirical, but it is claimed that they result in a significant improvement in the ability of this mechanistic approach to represent the observed vapour fluxes.

CONCLUSIONS

An investigation of vapour movement in unsaturated bentonite has been described. In particular, vapour fluxes have been quantified and compared with existing mechanistic theories.

A thermo-hydraulic cell has been used to allow thermal gradients to be applied to confined soil samples. The cell is capable of measuring the transient temperature, and facilitates the determination of the moisture content, dry density and chemical composition (anion and cation concentration) of the soil samples at the end of the tests. Undertaking a series of tests of different durations allows pseudo-transient results to be measured.

Results of a series of thermal gradient tests on both relatively dry and wet samples of MX-80 bentonite are presented. In each test thermal equilibrium is reached rapidly, with moisture content and porosity progressively decreasing in the warmer regions and increasing in the cooler regions. Soluble chloride ion accumulation near the heater surface indicates advective movement of this conservative ion and the establishment of a cycle of moisture movement away from the warmer regions in the vapour phase, condensation in the cooler regions, and a subsequent movement of liquid back towards the warmer regions.

An empirical method has been applied to calculate the vapour fluxes, using the variation of soluble chloride ions concentration and moisture content with time. The vapour

fluxes calculated empirically are found to be lower than those determined by some existing vapour flow theories. Subsequently, an existing vapour flow model was modified to achieve an improved representation of the observed vapour fluxes.

The experimental results and the subsequent estimation of vapour fluxes allow the direct quantification of the material parameters required for the mechanistic models of vapour fluxes typically used in THM and thermo-hydraulic-chemical-mechanical formulations. It is claimed that this quantification removes one of the remaining uncertainties in calculation of both resaturation times for geological waste repositories and advective chemical fluxes in thermal-hydraulic systems.

#### ACKNOWLEDGEMENTS

This research work was jointly sponsored by the EC under project FI6W-CT-2003-02389 (NF-Pro) and the Nuclear Decommissioning Authority; this financial support is gratefully acknowledged. The authors are also thankful to Dr Nam Young Do and Len Czekaj's contribution during the design and construction of the test cell.

#### NOTATION

$C$	concentration
$D_{\text{atms}}$	molecular diffusivity of vapour through air
$g$	gravitational constant
$h$	relative humidity
$m$	mass of chloride ions
$n$	porosity
$P_{\text{atm}}$	atmospheric pressure
$P_g$	pore gas pressure
$P_0$	fitting parameter
$q_v$	vapour flux
$R_v$	specific gas constant for vapour
$S_{\text{e}}$	effective degree of saturation
$S_{\text{r}}$	residual degree of saturation
$S_{\text{is}}$	maximum degree of saturation
$s$	suction
$T$	temperature
$T_0$	reference temperature
$t$	time
$V$	volume of liquid
$\theta$	volumetric moisture content
$\theta_a$	volumetric air content
$\lambda$	fitting parameter
$\nu_v$	mass flow factor
$\xi$	surface energy of soil water
$\rho_v$	vapour density
$\rho_0$	saturated vapour density
$\tau_v$	tortuosity factor
$\psi$	capillary potential

#### REFERENCES

- Börgesson, L., Chijimatsub, M., Fujitab, T., Nguyenc, T. S., Rutqvist, J. & Jinge, L. (2001). Thermo-hydro-mechanical characterisation of a bentonite-based buffer material by laboratory tests and numerical back analyses. *Int. J. Rock Mech. Mining Sci.* **38**, No. 1, 95–104.
- BSI (1990). *Soils for civil engineering purposes. Part 2: Classification tests*, BS 1377-2. Milton Keynes, UK: British Standards Institution.
- Cleall, P. J., Seetharam, S. C. & Thomas, H. R. (2007). Inclusion of some aspects of chemical behaviour of unsaturated soil in thermo/hydro/chemical/mechanical models. I: Model development. *ASCE J. Engng Mech.* **133**, No. 3, 338–347.
- Cleall, P. J., Singh, R. M. & Thomas, H. R. (2011). Non-isothermal moisture movement in unsaturated kaolin: an experimental and theoretical investigation. *ASTM Geotech. Test. J.* **34**, No. 5, 514–524.
- Edlefsen, N. E. & Anderson, A. B. C. (1943). Thermodynamics of soil moisture. *Hilgardia* **15**, No. 2, 31–298.
- Ewen, J. & Thomas, H. R. (1989). Heating unsaturated medium sand. *Géotechnique* **39**, No. 3, 455–470, <http://dx.doi.org/10.1680/geot.1989.39.3.455>.
- Gatabin, C. & Billaud, P. (2005). *Bentonite THM mock up experiments: Sensors data report*, Report NT-DPC/SCCME 05-300-A. Paris, France: CEA.
- Gens, A. (2010). Soil–environment interactions in geotechnical engineering. *Géotechnique* **60**, No. 1, 3–74, <http://dx.doi.org/10.1680/geot.9.P.109>.
- Gómez-Espina, R. & Villar, M. V. (2010). Geochemical and mineralogical changes in compacted MX-80 bentonite submitted to heat and water gradients. *Appl. Clay Sci.* **47**, No. 3–4, 400–408.
- Kanno, T., Kato, K. & Yamagata, J. (1996). Moisture movement under a temperature gradient in highly compacted bentonite. *Engng Geol.* **41**, No. 1–4, 287–300.
- Lee, G., Glascoe, N. M., Wright, S. J. & Abriola, L. M. (1999). Modelling the influence of heat/moisture exchange during bioventing. *J. Environ. Engng ASCE* **125**, No. 12, 1093–1103.
- Luikov, A. V. (1966). *Heat and mass transfer in capillary porous bodies*. Oxford, UK: Pergamon.
- Madsen, F. T. (1998). Clay mineralogical investigations related to nuclear waste disposal. *Clay Miner.* **33**, No. 1, 109–129.
- Olivella, S. & Gens, A. (2000). Vapour transport in low permeability unsaturated soils with capillary effects. *Transp. Porous Media* **40**, No. 2, 219–241.
- Olivella, S., Gens, A., Carrera, J. & Alonso, E. E. (1996). Numerical formulation for a simulator (CODE\_BRIGHT) for the coupled analysis of saline media. *Engng Comput.* **13**, No. 7, 87–112.
- Philip, J. R. & de Vries, D. A. (1957). Moisture movement in porous materials under temperature gradients. *Trans. Am. Geophys. Union* **38**, No. 2, 222–232.
- Pintado, X., Ledesma, A. & Lloret, A. (2002). Backanalysis of thermohydraulic bentonite properties from laboratory tests. *Engng Geol.* **64**, No. 2–3, 91–115.
- Rees, S. W., Adjali, M. H., Zhou, Z., Davies, M. & Thomas, H.R. (2000). Ground heat transfer effects on the thermal performance of earth-contact structures. *Renew. Sustain. Energy Rev.* **4**, No. 3, 213–265.
- Singh, R. M. (2007). *An experimental and numerical investigation of heat and moisture movement in unsaturated clays*. PhD thesis, Cardiff University, UK.
- Tang, A.-M., Cui, Y.-J. & Le, T.-T. (2008). A study on the thermal conductivity of compacted bentonites. *Appl. Clay Sci.* **41**, No. 3–4, 181–189.
- Thomas, H. R. & He, Y. (1995). Analysis of coupled heat, moisture and air transfer in a deformable unsaturated soil. *Géotechnique* **45**, No. 4, 677–689, <http://dx.doi.org/10.1680/geot.1995.45.4.677>.
- Thomas, H. R. & Sansom, M. R. (1995). Fully coupled analysis of heat, moisture and air transfer in unsaturated soil. *ASCE J. Engng Mech.* **121**, No. 3, 392–405.
- US EPA (1994). *Test method for evaluating solid waste, physical/chemical methods (SW-846)*, US EPA 1312, 3rd edn, update 2B. EPA, Cincinnati, OH, USA: National Centre for Environmental Publications, United States Environmental Protection Agency.
- van Genuchten, M. T. (1980). A closed-form equation for predicting the hydraulic conductivity of unsaturated soils. *Soil Sci. Soc. Am. J.* **44**, No. 5, 892–898.
- Villar, M. V., Cuevas, J. & Martin, P. L. (1996). Effects of heat/water flow interaction on compacted bentonite: preliminary results. *Engng Geol.* **41**, No. 1–4, 257–267.
- Villar, M. V., Sánchez, M. & Gens, A. (2008). Behaviour of a bentonite barrier in the laboratory: experimental results up to 8 years and numerical simulation. *Phys. Chem. Earth* **33**, No. 1, 476–485.
- Yong, R. N. & Mohamed, A. M. O. (1996). Evaluation of coupled heat and moisture flow parameters in a bentonite-sand buffer material. *Engng Geol.* **41**, No. 1–4, 269–286.
- Yong, R. N., Mohamed, A. M. O., Shooshapasha, I. & Onofrei, C. (1997). Hydro-thermal performance of unsaturated bentonite-sand buffer material. *Engng Geol.* **47**, No. 4, 351–365.